Heliyon 10 (2024) e28584

Contents lists available at ScienceDirect

Heliyon

journal homepage: www.cell.com/heliyon

Research article

Artesunate induces ferroptosis by regulating MT1G and has an additive effect with doxorubicin in diffuse large B-cell lymphoma cells

Dan Xiong [a,*,1], Chengjie Geng [b,1], Liyi Zeng [b], Hua Yao [b], Jiewen Tan [a], Lan Zhang [b], Xiaohui Liu [b], Langxia Liu [b,**]

[a] *Department of Hematology, Shunde Hospital, Southern Medical University (The First People's Hospital of Shunde), Foshan, Guangdong, 528308, China*

[b] *MOE Key Laboratory of Tumor Molecular Biology and Key Laboratory of Functional Protein Research of Guangdong Higher Education Institutes, Institute of Life and Health Engineering, Jinan University, Guangzhou, 510632, China*

A B S T R A C T

Diffuse Large B-cell lymphoma (DLBCL) is a highly aggressive disease with heterogeneous outcomes and marked variability in the response to chemotherapy. DLBCL comprises two major subtypes: germinal centre B-cell-like (GCB) and activated B-cell-like (ABC). Our study highlights the extensive antitumour activity of artesunate (ART) against both major DLBCL subtypes. Transcriptome analysis suggests the potential involvement of ferroptosis in artesunate-induced cell death. Because of low glutathione (GSH) and glutathione peroxidase 4 (GPX4) levels, along with the accumulation of free iron (Fe^{2+}), artesunate induces the excessive production of reactive oxygen species (ROS), ultimately leading to ferroptosis, a form of cell death driven by phospholipid peroxidation. A putative target of artesunate, metallothionein 1G (MT1G), was selected for further analysis. Subsequent studies revealed that inhibiting MT1G expression *in vitro* significantly impedes the ferroptosis-promoting activity of artesunate by reducing lipid peroxidation and iron accumulation. We also showed that the combination of artesunate and doxorubicin had a marked additive inhibitory effect on GCB and ABC DLBCL cells. In conclusion, artesunate induces ferroptotic death in GCB and ABC DLBCL cells by attenuating the GPX4/GSH antioxidant defence system and increasing intracellular iron levels, indicating its therapeutic potential for relapsed or refractory DLBCL.

1. Introduction

Diffuse large B-cell lymphoma (DLBCL) is the most common malignant lymphoma in adults, and is characterised by an unusually rapid disease progression and aggressive clinical behavior. Gene expression profiling has identified two major DLBCL subtypes, germinal centre B-cell-like (GCB) and activated B-cell-like (ABC), which exhibit differential responses to chemotherapy and targeted therapies [1]. Despite the availability of first-line chemical immunotherapy R-CHOP, which includes rituximab, doxorubicin (Dox), cyclophosphamide, vincristine, and prednisone, approximately 40% of patients develop refractory disease or relapse within two years of the initial response [2,3]. Therefore, it is necessary to identify new therapeutic targets for relapsed or refractory DLBCL to develop more effective therapies.

Ferroptosis is an iron-dependent form of cell death that is morphologically, biochemically and genetically distinct from autophagy, necrosis, and apoptosis. The morphology of ferroptosis is characterised by mitochondrial density, reduction or disappearance of

* Corresponding author.
** Corresponding author.
E-mail addresses: xiongdancn@i.smu.edu.cn (D. Xiong), langxialiu@gmail.com (L. Liu).
[1] Equally contributed to this work.

https://doi.org/10.1016/j.heliyon.2024.e28584
Received 31 October 2023; Received in revised form 20 March 2024; Accepted 20 March 2024
Available online 22 March 2024
2405-8440/© 2024 The Authors. Published by Elsevier Ltd. This is an open access article under the CC BY-NC-ND license (http://creativecommons.org/licenses/by-nc-nd/4.0/).

mitochondrial cristae, and rupture of outer mitochondrial membrane (OMM). The lipid peroxide accumulation, metabolic dysfunction, and redox imbalance are considered distinct fingerprints of ferroptosis [4,5]. Mounting evidence indicates that activation of ferroptosis contributes to overcoming resistance to existing treatments [6]. Sensitivity analysis of 177 cancer cell lines showed that DLBCLs and renal cell carcinoma are particularly susceptible to ferroptosis regulated by glutathione peroxidase 4 (GPX4), however, the key regulators remain unknown [6].

Owing to the rising failure rate and high cost of developing new anticancer drugs, the role of traditional Chinese medicine in DLBCL treatment strategies has garnered attention. Song et al. demonstrated that artesunate, a drug commonly used to treat malaria, modulates two signalling pathways in glioblastoma cells: the p38 and ERK pathways. This modulation promotes the consumption of glutathione (GSH), a powerful antioxidant, and affects lipid peroxidation and iron overload in cells, thereby altering their susceptibility to ferroptosis [7]. This artesunate-mediated effect on ferroptosis may also be observed in DLBCL cells. We studied the effects of artesunate on GCB and ABC DLBCL cell lines and identified the underlying molecular biological mechanisms.

2. Materials and methods

2.1. Cell lines and cell culture, reagents, vectors

Riva, U2932, and OCI-ly8 DLBCL cell lines were purchased from ATCC American Type Culture Collection (Manassas, USA). These cells were kept in a 5% CO_2 incubator humidified in Dulbecco Modified Eagle Medium (DMEM) (Life Technologies, Gaithersburg, MD) containing 10% foetal bovine serum (FBS) (Life Technologies) at 37 °C. Erastin, Ferrostatin-1, and artesunate were purchased from MedChemExpress (Shanghai, China). Antibodies include: GPX4 (Cell Signalling Technology, Cat. 52455 S), GAPDH (Proteintech; Cat. 10494-1-AP), and horseradish peroxidase-conjugated goat anti-rabbit/mouse secondary antibodies (Jackson ImmunoResearch, PA, USA).

Lentiviral shRNA vectors against metallothionein 1G (MT1G) and the corresponding control vectors (constructed with the pLKO.1 vectors) were derived from Tsingke Biotech Co., Ltd. (Beijing, China). The sequences are as follows.

shMT1G #1	5′-CCGGGCCAGCTCCTGCAAGTGCAAACTCGAGTTTGCACTTGCAGGAGCTGGCTTTTTT-3′
sh MT1G #2	5′- CCGGCAAGTGCAAAGAGTGCAAATGCTCGAGCATTTGCACTCTTTGCACTTG-TTTTTT -3′
sh MT1G #3	5′-CCGGCCCAAGGCTGCATCTGCAAAGCTCGAGCTTTGCAGATGCAGCCTTGGGTTTTTT-3′
sh MT1G #4	5′-CCGGCTCCTGTGCCGCTGGTGTCTCCTCGAGGAGACACCAGCGGCACAGGAGTTTTTT-3′
control shRNA	5′-UUUGUACUACACAAAAGUACUG-3′

2.2. Detection of cell viability, cell death

Cell Counting Kit-8 (Beyotime, Shanghai, China) was used to evaluate cell viability. For the soft agar colony formation test, about 4 $\times 10^3$ cells in a soft agar mixture comprised of DMEM, 10% FBS, and 0.35% agarose were carefully overlaid onto a solidified 0.6% agar base and cultured for 2 weeks. The colonies were then immobilized and stained with nitrotetrazolium chloride blue (NBT) and counted after scanning. Cell death in DLBCL cells treated with or without artesunate was assessed by flow cytometry with propyl iodide (PI) staining (Beckman Coulter, Atlanta, USA) [8].

2.3. Determination of reactive oxygen species (ROS) levels

CM-H2DCFDA (GLPBIO, USA) were used for the detection of ROS [9]. In short, the cells were collected, gently washed, re-suspended in 1 mL phosphate-buffered saline (PBS), and then incubated in 5 mM H2DCFDA at 37 °C for 60 min. The cells labelled with fluorescent probes were centrifuged, the supernatant was discarded, and then re-suspended with PBS. Flow cytometry was used to analyse fluorescent signals.

2.4. Determination of lipid peroxidation

Detect lipid peroxidation using BODIPY 581/591C11 (GLPBIO, USA), as per manufacturer's instructions [10]. The relative concentration of glutathione in cell lysates was assessed using a glutathione assay kit (Solarbio, Beijing, China) according to the manufacturer's instructions. Malondialdehyde (MDA) content was quantified using a lipid peroxidation MDA assay kit (Beyotime, Shanghai, China) and a Multi-Mode Microplate Reader (BioTek, Vermont, USA).

2.5. Western blotting

The protein expression in the cells was analyzed by Western blotting as described previously [11]. Cell cultures were lysed and centrifuged to collect supernatants. The protein was determined using a BCA kit (Beyotime). The protein was isolated by 12% SDS-PAGE and transferred to polyvinylidene difluoride (PVDF) membranes (EMD Millipore, MA, USA). Then, the membranes were sequentially blocked in 5% dry skimmed milk at room temperature (RT) for 1 h, incubated with the primary antibodies at 4 °C

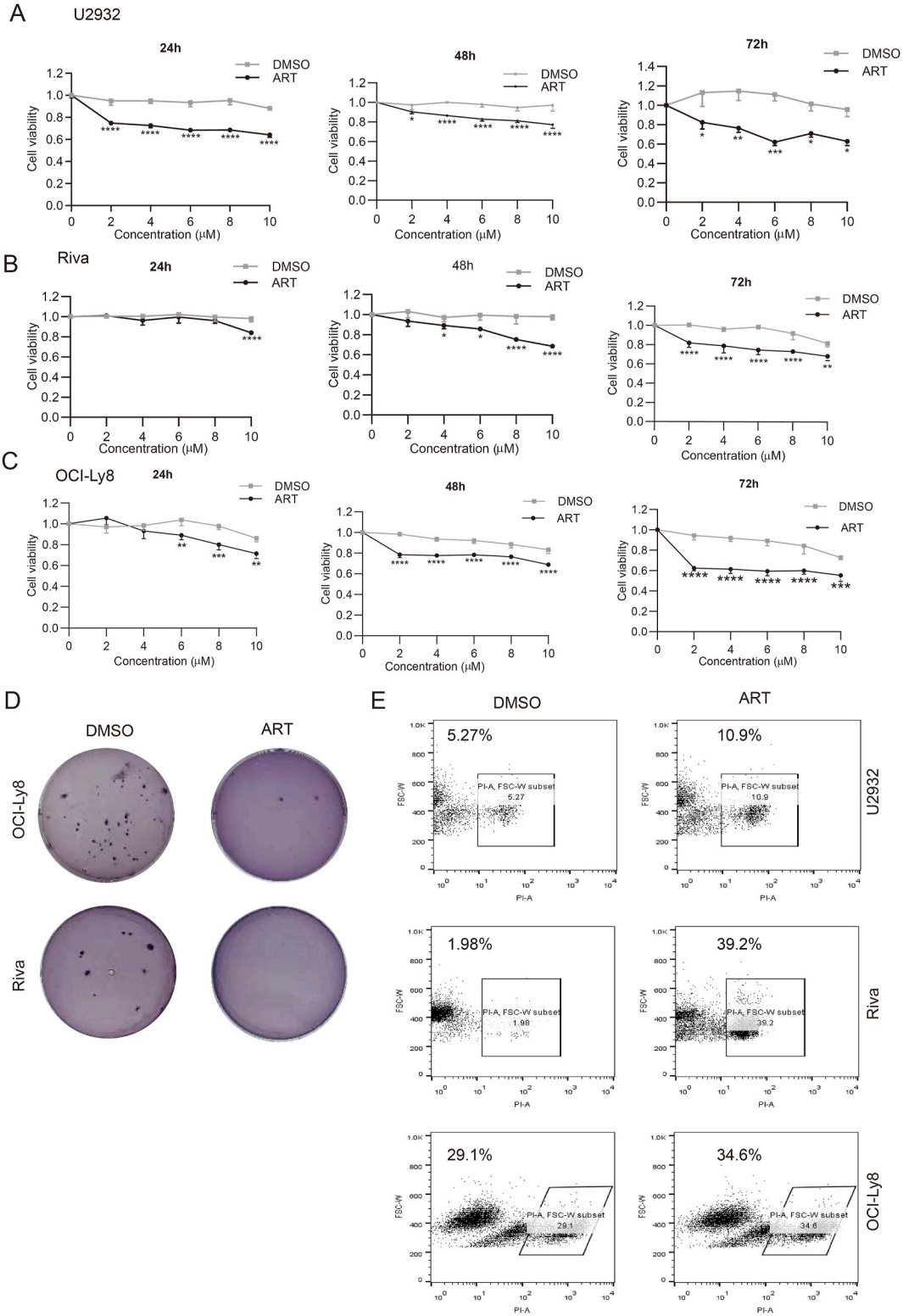

Fig. 1. Artesunate impairs DLBCL growth. (**A-C**) Cell proliferation determined by MTT assay under different doses of artesunate at the indicated time points. Data are presented as mean ± s.e.m. from three independent experiments. $^{**}p < 0.01$; $^{**}p < 0.001$, determined by two-way ANOVA. (**D**) The soft agar colony formation assay performed with indicated cells. (**E**) The cell survival rate was quantified by the PI staining assay. ART, artesunate.

overnight, and incubated with secondary antibodies at RT for 1 h. Protein expression was detected using an enhanced chemiluminescence kit (Beyotime).

2.6. Measurement of free Fe^{2+} ion levels

According to the manufacturer's instructions, the free Fe^{2+} ion levels in the cell lysates were determined using a FerroOrange Iron Assay Kit (Dojindo).

2.7. Experimental sample, RNA extraction, and RNA sequencing

U2932 cells were incubated with 100 μM artesunate or DMSO for 24 h in triplicate. Total RNA was extracted using TRIzol® Reagents (Invitrogen, CA, USA). Perform library preparation and RNA sequencing as previously described [12]. A total of six samples (three in the artesunate-treated group and three in the DMSO-treated group) were tested using the Illumina platform, and 95.35 Gb of data were obtained, in which the percentage of Q30 bases was 94.35% or above. The clean reads of each sample were sequenced against the specified reference genome, and the efficiency of the comparison ranged from 97.35% to 98.11%.

2.8. Identification of differentially expressed genes (DEGs)

Sequencing reads from Illumina NovaSeq 6000 were checked for quality using Fastp [13]. The total clean data of the sequencing samples was 95.35 Gb, and the average proportion of Q30 was above 94.35%. The EdgeR software package was used to analyse DEGs in paired samples [12]. Absolute value of log2 (fold-change, FC) > 1 and false discovery rate (FDR) < 0.01 were designated as differentially expressed. Then, use the DAVID (https://david.ncifcrf.gov/) tool for Gene Ontology (GO) functional enrichment and Kyoto Encyclopedia of Genes and Genomes (KEGG) pathway enrichment analyses of the DEGs.

2.9. Real-time fluorescence quantitative PCR (qRT-PCR)

Real-time fluorescence quantitative PCR was performed according to the manufacturer's instructions using SYBR Green Supermix (Bio-Rad, Hercules, USA) [11]. The internal control gene was GAPDH. The primers were listed below.

primers	Sequence	Tm
MT1G-F	5′-CAAGTGCAAAGAGTGCAAA-3′	51 °C
MT1G-R	5′-CCTGGATTTTACGGGTCA-3′	51 °C
FTL-F	5′- CAGCCTGGTCAATTTGTACCT-3′	55 °C
FTL-R	5′- GCCAATTCGCGGAAGAAGTG-3′	57 °C
TFRC-F	5′- ACCTGTCCAGACAATCTCCAG-3′	56 °C
TFRC-R	5′- TGTTTTCCAGTCAGAGGGACA-3′	56 °C
STEAP3-F	5′- TGCAAACTCGCTCAACTGGAG-3′	58 °C
STEAP3-R	5′- GAAGGTGGGAGGCAGGTAGAA-3′	59 °C
GAPDH-F	5′-GTCTCCTCTGACTTCAACAGCG-3′	58 °C
GAPDH-R	5′-ACCACCCTGTTGCTGTAGCCAA-3′	60 °C

2.10. Statistical analysis

All experiments were repeated in triplicates in three independent experiments. A negative binomial distribution was used for RNA-Seq, and the Benjamin-Hochberg method was used to adjust the *p*-value. Fold-change in gene expression from qRT-PCR assay was calculated using $2^{-\Delta\Delta ct}$ [11]. Two-tailed Student's t-test was used to analyse the significant differences between the two groups, and two-way analysis of variance (ANOVA) was used to analyse significant differences between the multiple groups. p values < 0.05 was considered as statistically significant.

3. Results

3.1. Artesunate impairs DLBCL growth

Artesunate decreased the viability of representative ABC DLBCL (Riva, U2932) and GCB (OCI-ly8) DLBCL cell lines in a dose-dependent manner. U2932 cells were more sensitive to artesunate than Ly8 within 24 h; whilst Ly8 cells were more sensitive to artesunate than ABC-type DLBCL cells after 24 h (Fig. 1A–C). The results of soft agar colony formation assay showed a significant decrease in Ly8 and Riva cells treated with artesunate compared to that in cells treated with DMSO. Representative micrographs of artesunate-induced cell growth inhibition are shown in Fig. 1D. The results of flow cytometry analysis further confirmed that artesunate-induced cell death in both the representative ABC and GCB DLBCL cell lines (Fig. 1E).

Gene differential expression profiling analysis suggests that ferroptosis may be involved in artesunate-induced DLBCL cell death.

To explore the underlying mechanism of artesunate-induced DLBCL cell death, RNA sequencing was performed to identify DEGs in artesunate-treated U2932 cells. A total of 1987 DEGs were identified, with 955 significantly upregulated genes and 1032 significantly downregulated genes (Fig. 2A). Functional enrichment analysis by KEGG showed that these DEGs participated mainly in protein processing in the endoplasmic reticulum (e.g. ERO1A, ERO1B, TRAM1, UBXN1, HSP90AB1), DNA replication (e.g. RFC5, RNASEH2C, RFC3, RNASEH2A, PCNA), ferroptosis (e.g. STEAP3, TFRC, ACSL3, FTH1, FTL), mineral absorption (e.g. FTH1, MT1F, MT1G, HMOX1, MT1H), and measles (e.g. CDKN1B, TRADD, PIK3CD, PIK3R3, PIK3R2). Among the 30 most significant pathways, ferroptosis ranked third, indicating that artesunate may have had a significant impact on this pathway (Fig. 2B). Furthermore, gene set enrichment

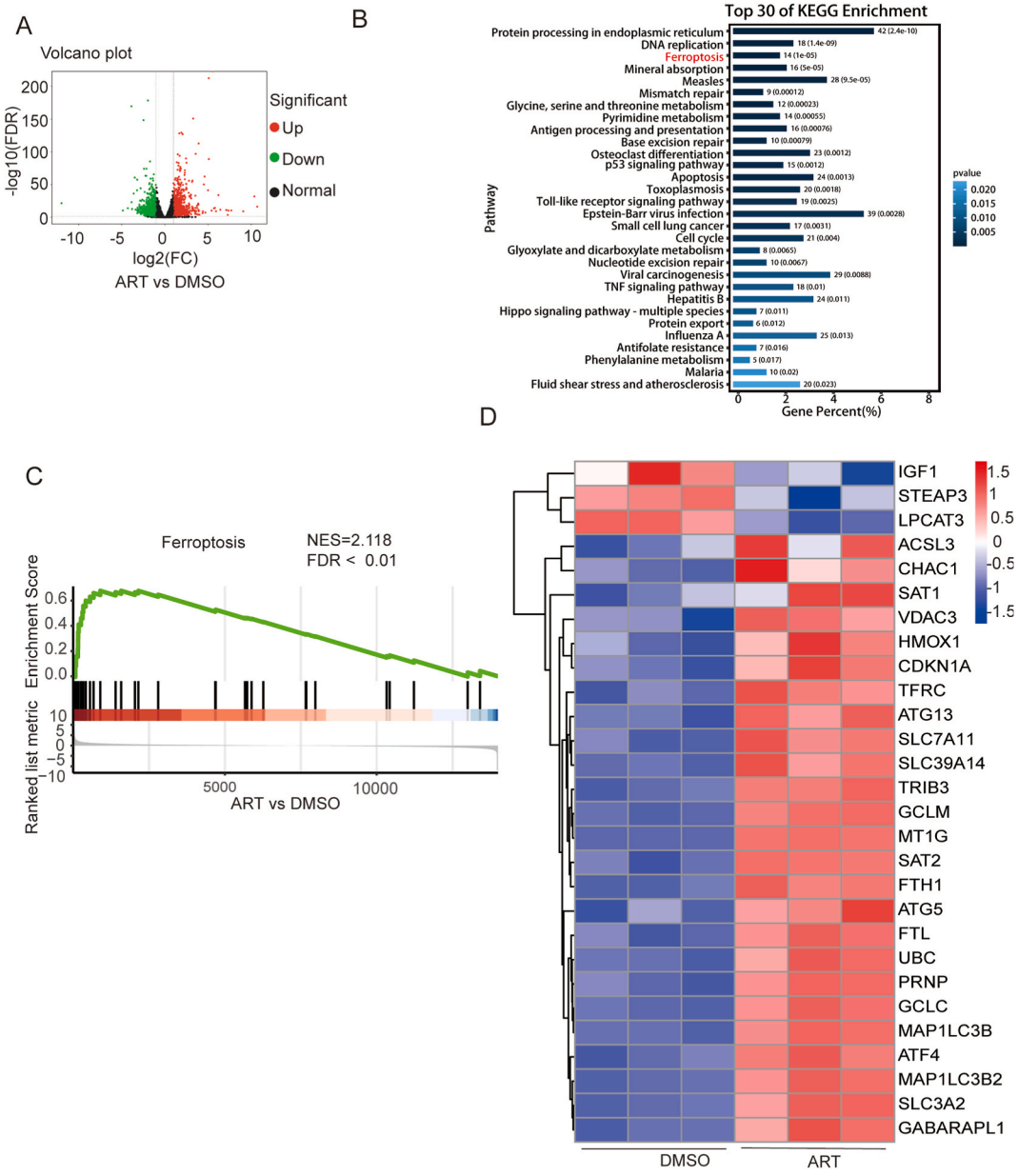

Fig. 2. Gene differential expression profiling analysis suggests that ferroptosis may be involved in artesunate induced DLBCL cell death. (**A**) Volcano plot of global DEGs between U2932 cells treated with 100 μM artesunate for 24 h and their corresponding control cells. (**B**) The functions of DEGs were predicted by analysis of KEGG by DAVID (https://david.ncifcrf.gov/). (**C**) GSEA enrichment analysis. The green curve represents the dynamic enrichment score (ES) value, and the highest point represents the ES value of this feature. The bar code in the middle indicates the location of genes in the genome. NES represents normalized ES value. FDR represents *p*-value after correction for multiple testing, and FDR<0.01 were considered statistically significant. (**D**) Heat map of differentially expressed genes for ferroptosis. Red represents up-regulated genes, blue represents down-regulated genes. C and D are based on KEGG pathway (https://www.genome.jp/entry/map04216). (For interpretation of the references to colour in this figure legend, the reader is referred to the Web version of this article.)

analysis (GSEA) showed significant enrichment of ferroptosis after artesunate treatment (Fig. 2C). Heat maps showed that genes associated with ferroptosis were generally highly expressed in the artesunate-treated group (Fig. 2D).

3.2. Artesunate augments cellular ROS production in DLBCL cells

The production of ROS and subsequent hydroxyl radical (·OH) mediated lipid peroxidation that ultimately leads to plasma membrane damage are the core events leading to ferroptosis. KEGG pathway enrichment analysis and GSEA were used to predict ferroptosis pathways. To verify whether artesunate-induced DLBCL cell death is ferroptotic cell death, we first examined the levels of ROS in Riva and U2932 cells treated with progressively increased artesunate concentration for 24 h, and ROS levels were measured. As shown in Fig. 3A and B, compared with the control group, the peak in the artesunate-treated group shifted significantly to the right, and the fluorescence intensity increased in a concentration-dependent manner. Together, these results indicated that artesunate markedly increased ROS generation in DLBCL cells.

3.3. Artesunate induces ferroptotic cell death in DLBCL cells

To confirm whether an increase in ROS levels causes lipid peroxidation in DLBCL cells, we used a C11-BODIPY 581/591 fluorescent probe to detect lipid peroxidation in artesunate-treated DLBCL cells. Riva, U2932, and OCI-ly8 cells were treated with 25 μM, 50 μM, 100 μM, or 150 μM artesunate for 24 h, and lipid peroxidation levels were measured. The results showed that artesunate markedly

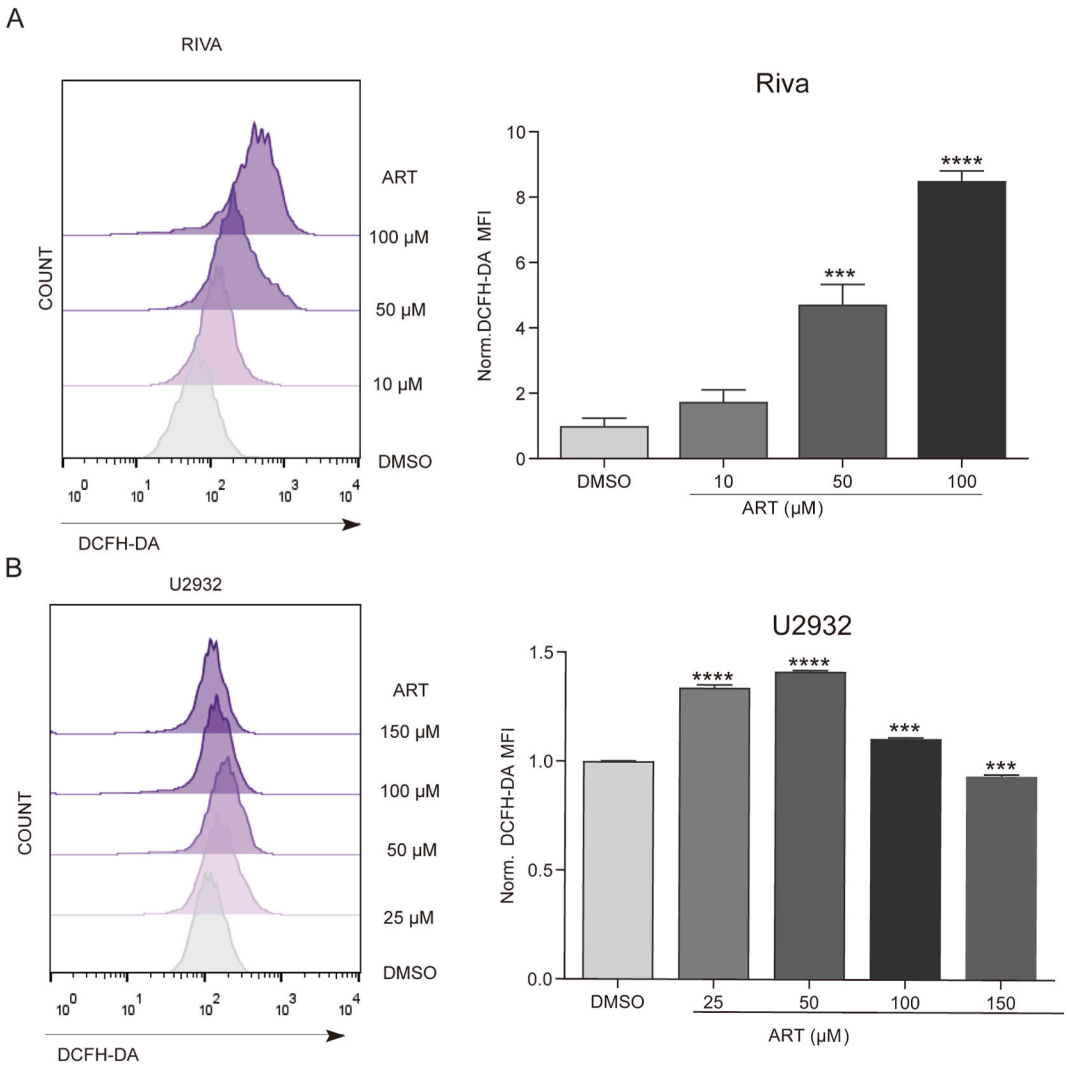

Fig. 3. Artesunate augments cellular ROS production in DLBCL cells. Total ROS (DCF-DA) measurements in Riva (**A**), and U2932 (**B**) cells treated with indicated concentrations of artesunate. Data are presented as mean ± s.d. from three independent experiments. Statistical significance was calculated using two-way ANOVA with Tukey's multiple comparison. ***$p < 0.001$ and ****$p < 0.0001$.

induced lipid peroxidation in a concentration-dependent manner (Fig. 4A and B). Furthermore, MDA, the end products of lipid peroxidation [14], was significantly decreased after treatment with artesunate in Riva, U2932, and OCI-ly8 cells (Fig. 4C). U2932 cells were treated with 50 μM artesunate, in combination with increasing doses of Ferrostatin-1 (Fer-1), a ferroptosis inhibitor. Fer-1 was found to rescue artesunate-induced lipid peroxidation (Fig. 4D). Consistently, lipid peroxidation induced by artesunate at different concentrations was significantly attenuated by 25 μM Fer-1 (Fig. 4E). These results indicate that artesunate induces ferroptotic cell death in both ABC and GCB DLBCL cells.

3.4. Artesunate weakens GPX4/GSH antioxidant defence system in DLBCL cells

GPX4 utilizes GSH as a cofactor to decrease lipid peroxidation, thereby inhibiting ferroptosis in somatic cells [6]. The TCGA

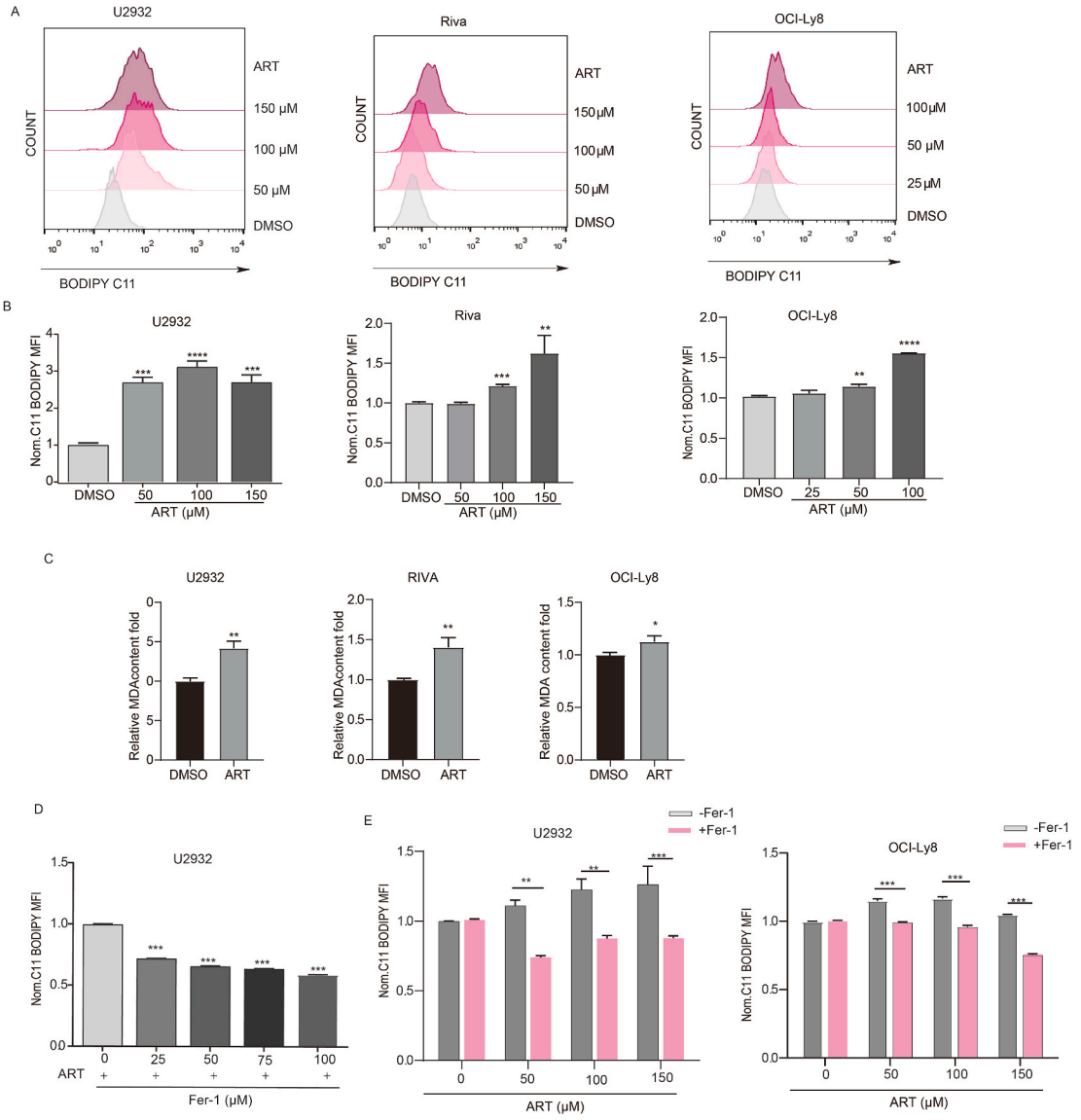

Fig. 4. Artesunate induces ferroptotic cell death in DLBCL cells. (**A-B**) Riva, U2932 and OCI-ly8 cells were treated with indicated concentrations of artesunate for 24 h and then stained with 5 μM C11-BODIPY followed by flow cytometry after 8 h treatment. (**C**) Riva, U2932 and OCI-ly8 cells were exposed to 100 μM artesunate for 24 h, Indicated DLBCL cells were treated with artesunate (100 μM) for 24 h and MDA levels were assayed. (**D**) U2932 cells were incubated overnight with 100 μM artesunate, then treated with indicated concentrations of Fer-1 for 6 h, then lipid ROS (5 μM C11-BODIPY) was detected by flow cytometry. Fer-1, Ferrostatin-1. (**E**) U2932 and OCI-ly8 cells were exposed to the indicated concentrations of artesunate with and or without Fer-1 (50 μM) for 24 h, then the lipid ROS (C11-BODIPY) was detected by flow cytometry. The mean ± s.d. values for three biological replicates are shown. Asterisks indicate statistically significant differences based on two-way ANOVA with Tukey's multiple comparison (**$p < 0.01$, and ***$p < 0.001$).

database showed that the expression of GPX4 mRNA in patients with DLBCL was higher in tumour tissues than in normal tissues, suggesting that DLBCL tumour tissues may have a higher antioxidant defence system to resist ferroptosis, which is conducive to tumour growth (Fig. 5A). We confirmed that artesunate induces lipid peroxidation in DLBCL cells. Western blot analysis showed that the protein levels of GPX4 were significantly downregulated in artesunate- or Erastin-treated U2932 cells, whereas this effect was markedly blocked by co-incubation with the ferroptosis inhibitor, Fer-1 (Fig. 5B). Furthermore, reduced GSH was significantly depleted by artesunate treatment in both ABC and GCB DLBCL cells (Fig. 5C). These results suggest that artesunate promotes ferroptosis in DLBCL cells by weakening the GPX4/GSH antioxidant defence system.

3.5. Artesunate induces iron overload in DLBCL cells

Given that ferrous iron (Fe^{2+}) plays an essential role in ferroptosis via the Fenton reaction and subsequent ROS production, we investigated whether artesunate affected iron metabolism [15]. Transferrin receptor (TFRC) mRNA levels were upregulated and ferritin heavy chain (FTH) mRNA levels were downregulated in response to artesunate treatment, although the mRNA levels of ferrireductase six-transmembrane epithelial antigen of prostate 3 (STEAP3) were not affected (Fig. 6A). Artesunate and erastin, classical ferroptotic inducers, significantly increased the levels of Fe^{2+} in U2932 cells at 6 h and 12 h. This effect was blocked by co-incubation with the iron chelator bipyridine (BPY) pretreatment (Fig. 6B). Collectively, these findings suggested that artesunate contributes, at least in part, to ferroptosis by regulating iron metabolism.

3.6. Artesunate-mediated DLBCL cell death in vitro is MT1G dependent

Our previous study identified 19 survival-related genes associated with ferroptosis [16]. Venn diagrams were used to visualise the overlapping genes between artesunate-regulated DEGs and survival-related genes. Six DEGs (MT1G, UBC, CHAC1, ATF4, GABARAPL1, and TRIB3) were selected for verification, and the mRNA expression level of MT1G was observed to be significantly increased by artesunate treatment (Fig. 7A and B). To determine whether increased MT1G expression plays a crucial role in artesunate's anticancer activity, four different shRNAs targeting MT1G were transfected into U2932 cells. As expected, the inhibition of MT1G expression by

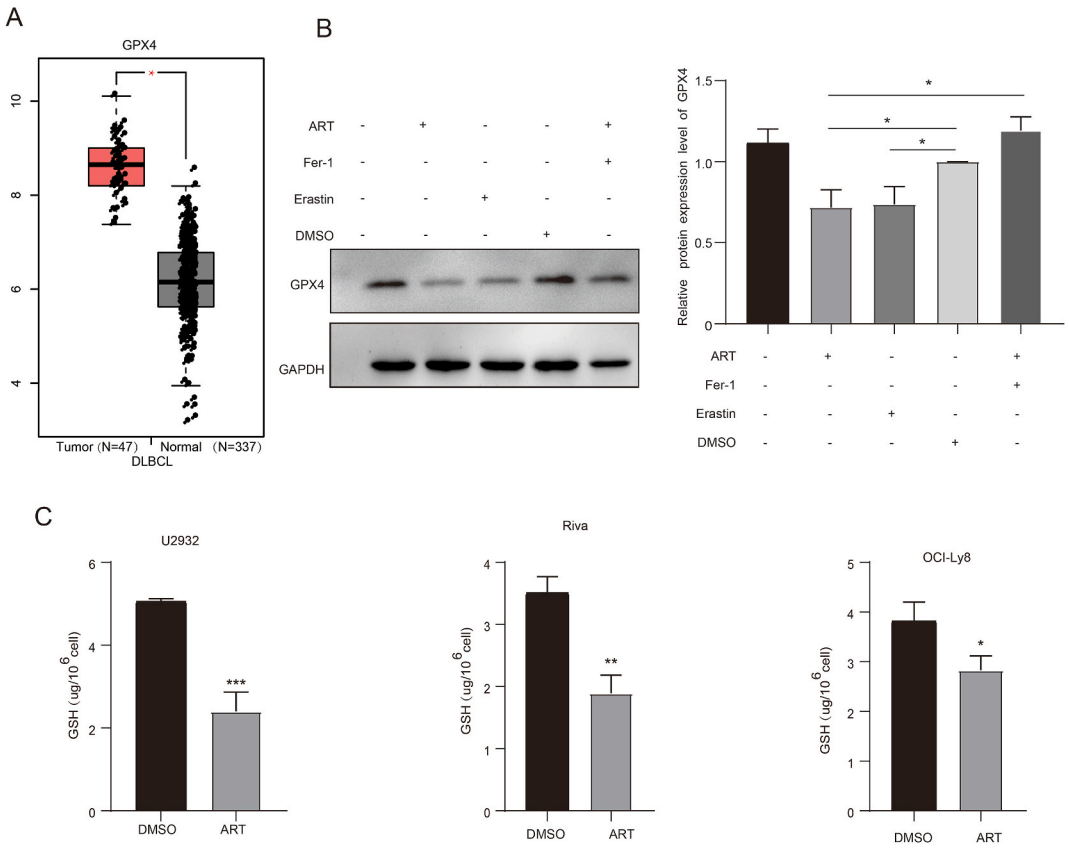

Fig. 5. Artesunate weakens GPX4/GSH antioxidant defense system in DLBCL cells. (**A**) The expression of GPX4 in patients with DLBCL (GEPIA, http://gepia.cancer-pku.cn/). (**B**) U2932 cells were treated with erastin (10 μM), artesunate (100 μM), and Fer-1 (20 μM) for 24 h and GPX4 protein levels were assayed. The uncropped image of blots can be obtained from supplementary materials. (**C**) The depletion of GSH by artesunate in U2932, Riva, and OCI-ly8 cells.

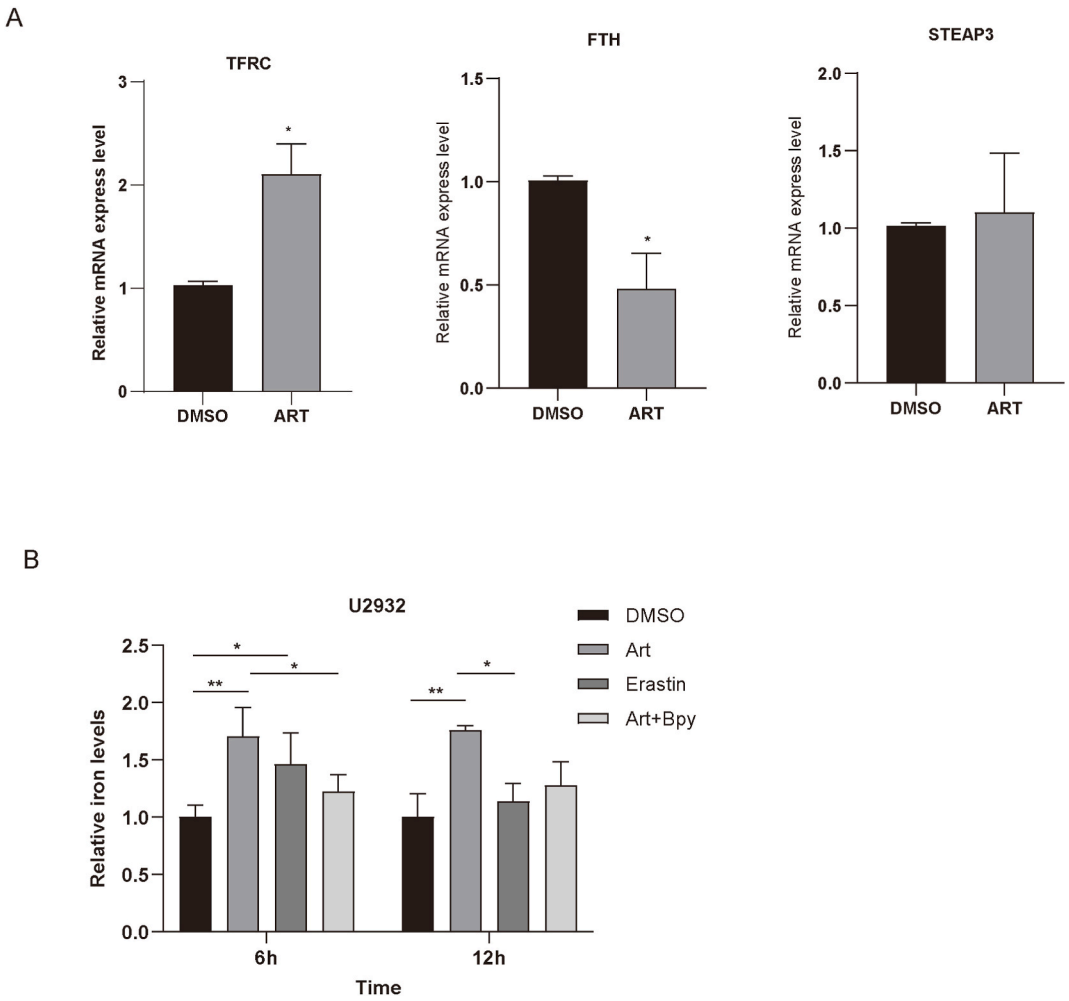

Fig. 6. Artesunate induces iron overload in DLBCL cells. (**A**) U2932 cells were treated with or without artesunate (100 μM) for 24 h, then mRNA levels of TFRC, FTH, and STEAP3 were assayed. Data are presented as mean ± s.d. *$p < 0.05$, determined by two-tailed Student's t-tests. (**B**) U2932 cells were treated with artesunate (100 μM), erastin (10 μM), or artesunate (100 μM) combined with BPY (5 μM) for 6 h or 12 h, respectively, and iron levels were detected. Data are presented as mean ± s.d. from three independent experiments. Statistical significance was calculated using two-way ANOVA with Tukey's multiple comparison. *$p < 0.05$ and **$p < 0.01$.

shRNA (Fig. 7C and D) significantly attenuated the anticancer effects of artesunate, as evidenced by the recovery of cell viability. The PI exclusion assay further demonstrated that suppression of MT1G expression inhibited artesunate-induced U2932 cell death, suggesting that suppression of MT1G expression inhibited artesunate antitumour sensitivity in DLBCL cells (Fig. 7E). The end products of lipid peroxidation, such as MDA, were significantly decreased following artesunate treatment in MT1G knockdown cells (Fig. 7F). Compared to control shRNA cells, artesunate treatment decreased the levels of Fe^{2+} in MT1G knockdown cells (Fig. 7G). Collectively, these findings indicated that MT1G is a central regulator of artesunate-induced ferroptotic cell death.

3.7. Artesunate combined with Dox further decreased cell viability

The first-line chemotherapy drug Dox has serious side effects, particularly cardiotoxicity, which limits its availability for DLBCL [3]. We hypothesised that artesunate may act synergistically with Dox to inhibit DLBCL. Different concentrations of Dox in combination with or without artesunate (100 μM) were added to U2932 cells and incubated for 24 h, 48 h, 72 h, respectively. Subsequently, cell viability was evaluated by a CCK8 assay. The results showed that the combination of Dox and artesunate exerted a stronger inhibitory effect on cell viability than Dox alone (Fig. 8A). The same effect was also evident in Riva and OCI-ly8 cells, and even Dox was administered at doses as low as 2–4 μM in ABC-type DLBCL cells, and 6–9 μM in GCB type DLBCL cells (Fig. 8B).

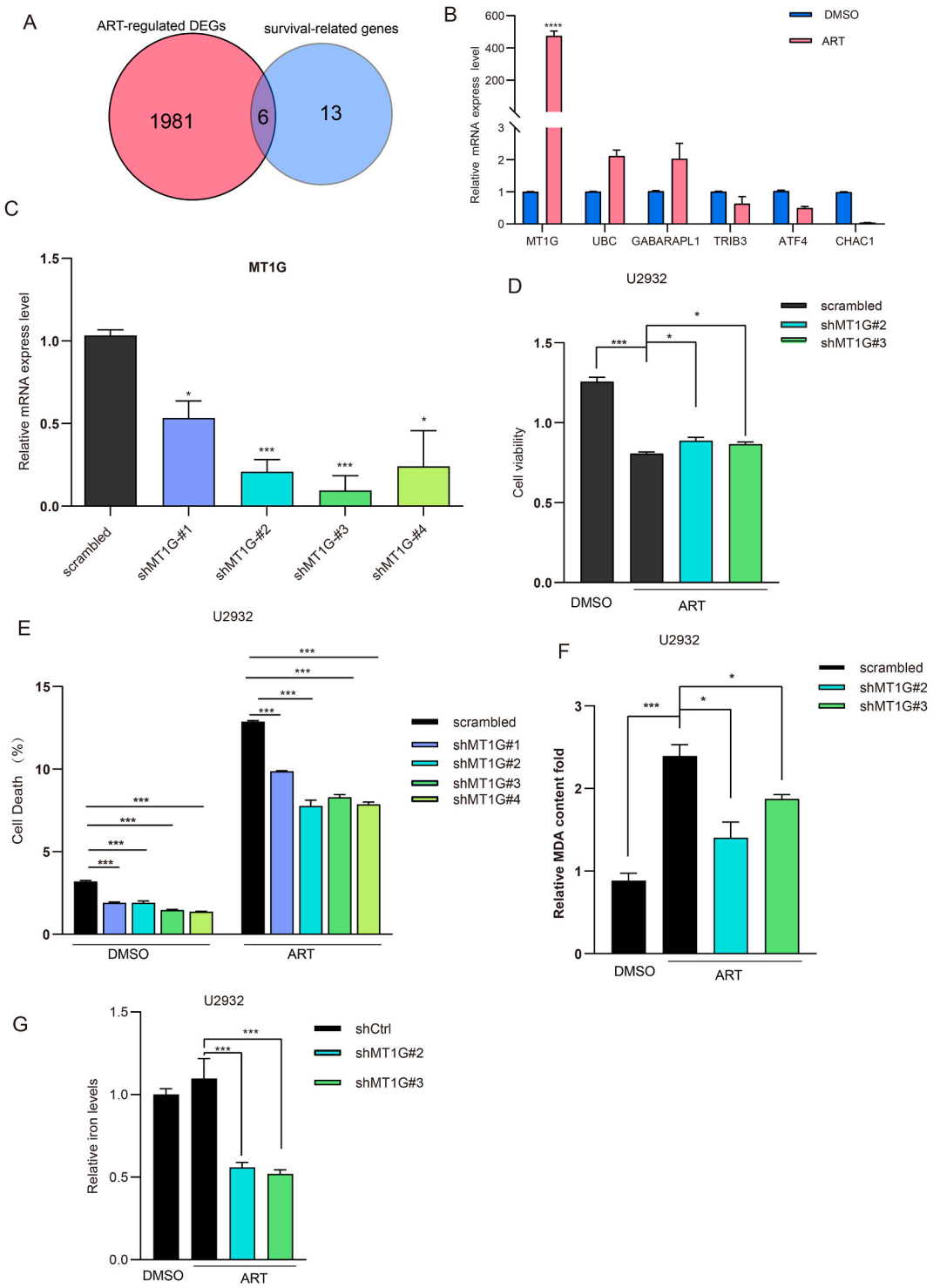

Fig. 7. Artesunate-mediated DLBCL cell death *in vitro* is MT1G dependent. (A) The Venn diagram of 19 ferroptosis-related prognostic genes and DEGs derived from transcriptome sequencing. (**B**) The fold-change of the relative mRNA expression levels in the 6 DEGs selected for qRT-PCR in U2932 cells treated with or without artesunate (100 μM). (**C**) MT1G stable knockdown in U2932 cells was verified by RT-qPCR assay. (**D**) MTT assays were performed in MT1G knockdown or control U2932 treated with or without artesunate (100 μM). Data are presented as mean ± s.d. from three independent experiments. $*p < 0.05$; $***p < 0.001$, determined by two-way ANOVA. Cell death (**E**), MDA (**F**) and iron measurements (**G**) in shRNA-mediated MT1G knockdown, or non-target scrambled U2932 cells treated with or without artesunate (100 μM). Data are presented as mean ± s.d. (B, C, D, E, F, and G). $*p < 0.05$, $**p < 0.01$, $***p < 0.001$, determined by two-way ANOVA.

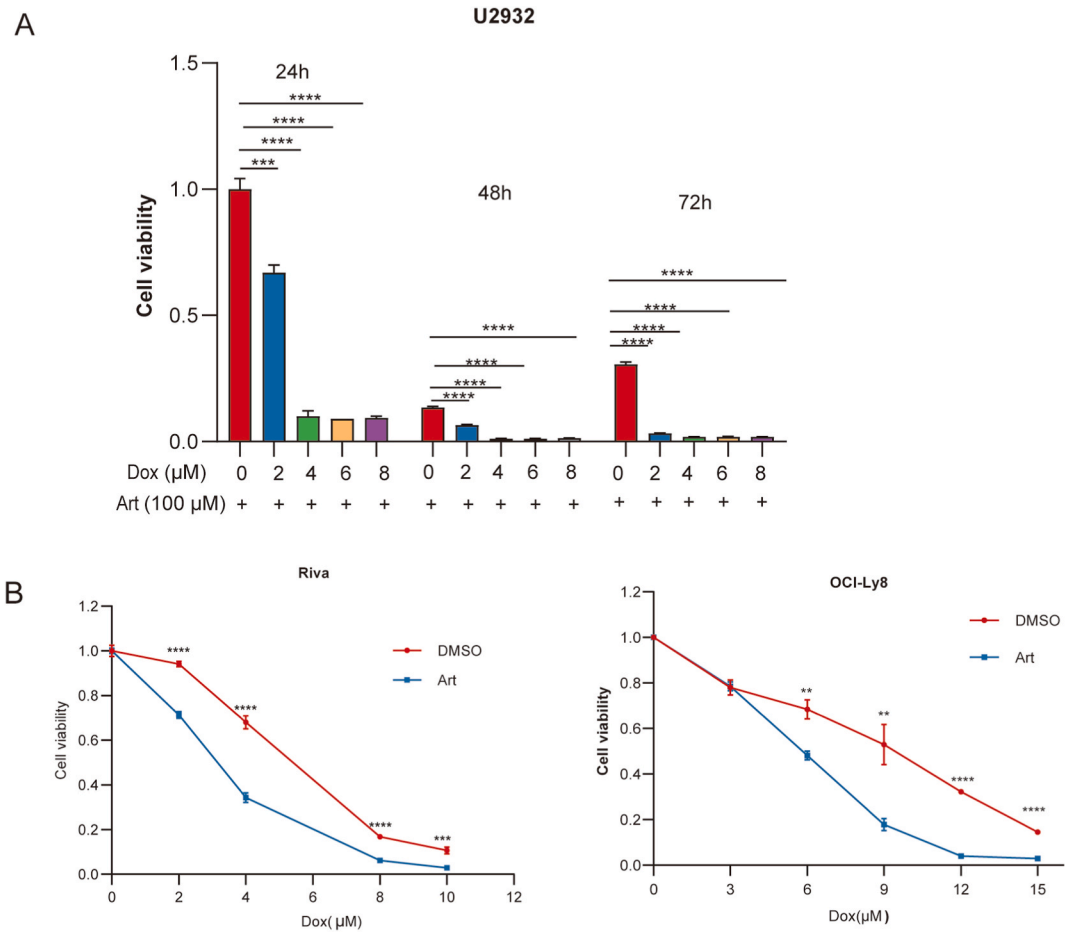

Fig. 8. Artesunate combined with Dox further decreased cell viability. U2932 cells (**A**) were exposed to increased concentrations of Dox with or without artesunate (100 μM) for 24 h, 48 h, and 72 h, while Riva and OCI-ly8 cells (**B**) were administered the same treatments for 24 h. Cell proliferation was detected by CCK8 assay.

4. Discussion

DLBCL originates from the malignant transformation of mature B lymphocytes in the secondary follicles of the germinal reaction of lymph nodes. It is a heterogeneous group of haematologic malignancies and is the most common pathological subtype of non-Hodgkin lymphoma (NHL) [17]. Approximately 25,000 new cases of DLBCL were diagnosed in the United States in 2020, representing approximately 30–40% of NHL patients worldwide [17,18]. The GCB subtype, which makes up approximately 40%–50% of DLBCL cases, and its gene expression profile is characterised by normal germinal centre B cells with intraconclonal heterogeneity, persistent high somatic mutation, and constitutive CD10 and BCL6 expression [19]. The ABC subtype, which accounts for 50%–60% of DLBCL, is characterised by post-germinal or activated B-cell gene expression with high expression and constituent activation of the nuclear factor kappa B (NF-κB) complex, and constitutive expression of B-cell lymphoma-2 (BCL-2) and interferon regulatory factor 4 (IRF4) [1,19]. Although the treatment of patients with DLBCL is of great interest to scientists, the current 5-year overall survival rate is 60%–70% using the existing R-CHOP regimen [2,3]. Therefore, exploring new targets for the treatment of DLBCL and finding more effective therapeutic approaches is essential [2,20,21].

Artesunate, a semisynthetic derivative of the first-line antimalarial drug artemisinin, is more clinically applicable because it is water-soluble, well-tolerated, and relatively inexpensive. Previous research results have demonstrated that artesunate can induce ferroptosis in certain types of cancers [7,22], research on its effects on DLBCL cells is limited. Recently, Chen et al. revealed that artesunate triggered ferroptosis in U2932 cells [23]. However, the underlying molecular regulatory mechanisms of ART-induced ferroptosis in DLBCL cells remain unclear. Here, we showed that artesunate significantly enhanced the anticancer effects in Riva, U2932, and OCI-ly8 cells by inducing lipid peroxidation, which could be blocked by ferroptosis inhibitors. The results of this study demonstrate the potential of artesunate as an effective and safe agent in treatment of patients with DLBCL. Sensitivity to ferroptosis induction varied between the two tested DLBCL cell subtypes. Notably, we found that ABC DLBCL with constitutively NF-kB activity appeared to be more susceptible to artesunate-regulated ferroptosis [24,25]. However, the killing effect of artesunate on the three

representative DLBCL cell lines was less than 50%, and there may be a mechanism that decreases artesunate sensitivity.

We used transcriptome analysis to comprehensively evaluate the mRNA changes that occurred upon artesunate treatment, in conjunction with prognostic analysis, to identify candidate target proteins for artesunate to improve DLBCL prognosis. The results of the RT-qPCR assay demonstrated that the mRNA level of MT1G significantly increased when subjected to artesunate treatment. These observations suggest that MT1G is a key factor in artesunate-mediated DLBCL cell death. MT1G is a member of the metallothionein family (MTs) that exhibits a high affinity for divalent heavy metal ions and plays a crucial role in protecting against heavy metals and oxidative damage [26–28]. Depending on the tumour type and stage, MTs have been thought to function as either oncogenes or tumour suppressor genes. Previous studies have provided limited information regarding the function of MT1G. However, Sun et al. showed that MT1G negatively regulates ferroptosis in hepatocellular carcinoma cells [29]. In contrast, our results demonstrated that suppression of MT1G expression in U2932 cells hindered the antitumour sensitivity of artesunate, suggesting an anti-survival role in tumour therapy. Moreover, we discovered that MT1G regulates intracellular lipid peroxidation and Fe^{2+} ion accumulation, thereby enabling artesunate to exert its ferroptosis-promoting activity. This suggests that MT1G has distinct functions depending on the specific cellular context. The identification of downstream interaction factors that could be used to analyse the contribution of each mode of action is needed to understand how MT1G exerts its biological activity and allow for eventual clinical use.

Preclinical evidence suggests that inducing ferroptotic cell death may be an effective strategy to overcome acquired resistance to several cancer therapies [30]. Dox, the main cytotoxic ingredient in R-CHOP, exerts its anticancer activity mainly by embedding itself in the DNA of cancer cells, inhibiting the action of topoisomerase II, and interfering with DNA synthesis and repair. Simultaneously, it destroys mitochondrial function, promotes the generation of free radicals, and promotes oxidative damage to cancer cells [31]. However, because of its short half-life and low bioavailability, high doses are often required to be effective, and high doses of Dox are often accompanied by serious side effects and toxicity, including cardiotoxicity, nephrotoxicity, and bone marrow suppression [32–34]. Our study showed that when artesunate was combined with Dox, an exciting additive effect was observed, which led to a potentiated anticancer effect. The mechanism underlying this additive effect has been hypothesised to be related to artesunate sensitising cancer cells by inducing ferroptosis, thereby making them more susceptible to the cytotoxic effects of Dox. However, the molecular mechanism of the additive effect of artesunate and Dox remains to be further explored.

In conclusion, artesunate can be easily translated into clinical applications owing to its good clinical tolerance, which will help improve the antitumour effect and prognosis of both GCB and ABC DLBCL.

5. Ethics approval and consent to participate

Not applicable.

Funding statement

This work was supported by grants from Guangdong Basic and Applied Basic Research Foundation (grant number: 2022A1515140022, 2023A1515010248, and 2023A1515011221); MOE Key Laboratory of Tumor Molecular Biology (202201), the medical Research Project of Shunde Hospital (grant no. SRSP2021038).

Data availability statement

Sequence data of RNA-seq have been deposited into the GEO, with the entry (https://www.ncbi.nlm.nih.gov/geo/query/acc.cgi?acc=GSE260741). The datasets used and/or analyzed in this study are available from the corresponding author upon reasonable request.

CRediT authorship contribution statement

Dan Xiong: Conceptualization, Project supervision, Manuscript revision. **Chengjie Geng:** Project administration, Methodology, Data curation. **Liyi Zeng:** Methodology, Investigation, Formal analysis. **Hua Yao:** Software, Formal analysis. **Jiewen Tan:** Methodology. **Lan Zhang:** Methodology. **Xiaohui Liu:** Writing – original draft, Supervision. **Langxia Liu:** Conceptualization, Project supervision, Resources, Manuscript revision.

Declaration of competing interest

The authors declare that they have no known competing financial interests or personal relationships that could have appeared to influence the work reported in this paper.

Appendix A. Supplementary data

Supplementary data to this article can be found online at https://doi.org/10.1016/j.heliyon.2024.e28584.

References

[1] R. Schmitz, G.W. Wright, D.W. Huang, C.A. Johnson, J.D. Phelan, J.Q. Wang, S. Roulland, et al., Genetics and pathogenesis of diffuse large B-cell lymphoma, N. Engl. J. Med. 378 (2018) 1396–1407.
[2] S. Susanibar-Adaniya, S.K. Barta, Update on Diffuse large B cell lymphoma: a review of current data and potential applications on risk stratification and management, American journal of hematology 2021 96 (2021) 617–629.
[3] M.R. Berendsen, W.B.C. Stevens, M. van den Brand, J.H. van Krieken, B. Scheijen, Molecular genetics of relapsed diffuse large B-cell lymphoma: insight into mechanisms of therapy resistance, Cancers 12 (2020).
[4] X. Jiang, B.R. Stockwell, M. Conrad, Ferroptosis: mechanisms, biology and role in disease, Nat. Rev. Mol. Cell Biol. 22 (2021) 266–282.
[5] M.M. Capelletti, H. Manceau, H. Puy, K. Peoc'h, Ferroptosis in liver diseases: an overview, Int. J. Mol. Sci. 21 (2020).
[6] W.S. Yang, R. SriRamaratnam, M.E. Welsch, K. Shimada, R. Skouta, V.S. Viswanathan, J.H. Cheah, et al., Regulation of ferroptotic cancer cell death by GPX4, Cell 156 (2014) 317–331.
[7] Q. Song, S. Peng, F. Che, X. Zhu, Artesunate induces ferroptosis via modulation of p38 and ERK signaling pathway in glioblastoma cells, J. Pharmacol. Sci. 148 (2022) 300–306.
[8] C. Riccardi, I. Nicoletti, Analysis of apoptosis by propidium iodide staining and flow cytometry, Nat. Protoc. 1 (2006) 1458–1461.
[9] G. Hong, Z. Chen, X. Han, L. Zhou, F. Pang, R. Wu, Y. Shen, et al., A novel RANKL-targeted flavonoid glycoside prevents osteoporosis through inhibiting NFATc1 and reactive oxygen species, Clin. Transl. Med. 11 (2021) e392.
[10] A.A. Caro, S. Thompson, J. Tackett, Increased oxidative stress and cytotoxicity by hydrogen sulfide in HepG2 cells overexpressing cytochrome P450 2E1, Cell Biol. Toxicol. 27 (2011) 439–453.
[11] X. Liu, X. Huang, J. Ma, L. Li, H. Hu, J. Feng, X. Gao, et al., 3'untranslated regions (3'UTR) of Gelsolin mRNA displays anticancer effects in non-small cell lung cancer (NSCLC) cells, Am. J. Cancer Res. 11 (2021) 3857–3876.
[12] X. Liu, L. Li, C. Geng, S. Wen, C. Zhang, C. Deng, X. Gao, et al., DDX17 promotes the growth and metastasis of lung adenocarcinoma, Cell death discovery 8 (2022) 425.
[13] S. Chen, Y. Zhou, Y. Chen, J. Gu, fastp: an ultra-fast all-in-one FASTQ preprocessor, Bioinformatics 34 (2018) i884–i890.
[14] L.J. Niedernhofer, J.S. Daniels, C.A. Rouzer, R.E. Greene, L.J. Marnett, Malondialdehyde, a product of lipid peroxidation, is mutagenic in human cells, J. Biol. Chem. 278 (2003) 31426–31433.
[15] D.G. Liu, Q.H. Jiang, Y.Y. Wei, L. Sun, B.B. Fu, F.K. Zhao, Q. Zhou, Gene expression profile favoring phenotypic reversion: a clue for mechanism of tumor suppression by NF-IL6 3'UTR, Cell Res. 13 (2003) 509–514.
[16] D. Xiong, M. Li, C. Zeng, Construction and validation of a risk scoring model for diffuse large B-cell lymphoma based on ferroptosis-related genes and its association with immune infiltration, Transl Oncol 16 (2022) 101314.
[17] A. Carbone, S. Roulland, A. Gloghini, A. Younes, G. von Keudell, A. López-Guillermo, J. Fitzgibbon, Follicular lymphoma, Nat. Rev. Dis. Prim. 5 (2019) 83.
[18] R.L. Siegel, K.D. Miller, A. Jemal, Cancer statistics, 2020, CA A Cancer J. Clin. 70 (2020) 7–30.
[19] K. Basso, R. Dalla-Favera, Germinal centres and B cell lymphomagenesis, Nat. Rev. Immunol. 15 (2015) 172–184.
[20] P.F. Caimi, W. Ai, J.P. Alderuccio, K.M. Ardeshna, M. Hamadani, B. Hess, B.S. Kahl, et al., Loncastuximab tesirine in relapsed or refractory diffuse large B-cell lymphoma (LOTIS-2): a multicentre, open-label, single-arm, phase 2 trial, Lancet Oncol. 22 (2021) 790–800.
[21] N. Wang, G.Z. Zeng, J.L. Yin, Z.X. Bian, Artesunate activates the ATF4-CHOP-CHAC1 pathway and affects ferroptosis in Burkitt's Lymphoma, Biochem. Biophys. Res. Commun. 519 (2019) 533–539.
[22] J.-L. Roh, E.H. Kim, H. Jang, D. Shin, Nrf2 inhibition reverses the resistance of cisplatin-resistant head and neck cancer cells to artesunate-induced ferroptosis, Redox Biol. 11 (2017) 254–262.
[23] Y. Chen, F. Wang, P. Wu, S. Gong, J. Gao, H. Tao, Q. Shen, et al., Artesunate induces apoptosis, autophagy and ferroptosis in diffuse large B cell lymphoma cells by impairing STAT3 signaling, Cell. Signal. 88 (2021) 110167.
[24] A. Schmitt, W. Xu, P. Bucher, M. Grimm, M. Konantz, H. Horn, M. Zapukhlyak, et al., Dimethyl fumarate induces ferroptosis and impairs NF-κB/STAT3 signaling in DLBCL, Blood 138 (2021) 871–884.
[25] R. Shen, D. Fu, L. Dong, M.C. Zhang, Q. Shi, Z.Y. Shi, S. Cheng, et al., Simplified algorithm for genetic subtyping in diffuse large B-cell lymphoma, Signal Transduct. Targeted Ther. 8 (2023) 145.
[26] O.A. Adebambo, P.D. Ray, D. Shea, R.C. Fry, Toxicological responses of environmental mixtures: environmental metal mixtures display synergistic induction of metal-responsive and oxidative stress genes in placental cells, Toxicol. Appl. Pharmacol. 289 (2015) 534–541.
[27] M. Si, J. Lang, The roles of metallothioneins in carcinogenesis, J. Hematol. Oncol. 11 (2018) 107.
[28] M. Lappas, Expression and regulation of metallothioneins in myometrium and fetal membranes, American journal of reproductive immunology (New York, NY 2018 (1989) e13040, 80.
[29] X. Sun, X. Niu, R. Chen, W. He, D. Chen, R. Kang, D. Tang, Metallothionein-1G facilitates sorafenib resistance through inhibition of ferroptosis, Hepatology 64 (2016) 488–500.
[30] X. Chen, R. Kang, G. Kroemer, D. Tang, Broadening horizons: the role of ferroptosis in cancer, Nat. Rev. Clin. Oncol. 18 (2021) 280–296.
[31] Y. Mai, J.J. Yu, B. Bartholdy, Z.Y. Xu-Monette, E.E. Knapp, F. Yuan, H. Chen, et al., An oxidative stress-based mechanism of doxorubicin cytotoxicity suggests new therapeutic strategies in ABC-DLBCL, Blood 128 (2016) 2797–2807.
[32] S. Chen, J. Chen, W. Du, D.M. Mickelsen, H. Shi, H. Yu, S. Kumar, et al., PDE10A inactivation prevents doxorubicin-induced cardiotoxicity and tumor growth, Circ. Res. 133 (2023) 138–157.
[33] A.I. Abushouk, A. Ismail, A.M.A. Salem, A.M. Afifi, M.M. Abdel-Daim, Cardioprotective mechanisms of phytochemicals against doxorubicin-induced cardiotoxicity, Biomedicine & pharmacotherapy = Biomedecine & pharmacotherapie 90 (2017) 935–946.
[34] F.S. Carvalho, A. Burgeiro, R. Garcia, A.J. Moreno, R.A. Carvalho, P.J. Oliveira, Doxorubicin-induced cardiotoxicity: from bioenergetic failure and cell death to cardiomyopathy, Med. Res. Rev. 34 (2014) 106–135.